IJCRT.ORG ISSN : 2320-2882

INTERNATIONAL JOURNAL OF CREATIVE RESEARCH THOUGHTS (IJCRT)

An International Open Access, Peer-reviewed, Refereed Journal

INVESTIGATIONS ON STRUCTURAL AND FUNCTIONAL PROPERTIES OF ZINC-COBALT FERRITE NANOPARTICLES

D. Chinna Venkata Subbaiah[1], Dr.S Dastagiri[2*], Prof. G.Pakardin[3**], Kongi Prasad[1], P.Ameena[1], Dr.K.Evangili Supriya[2] and Prof. MV Lakshmaiah[2]

[1]Department of Physics, Yogi Vemana University, YSR Kadapa, A.P., India,
[2]Department of Physics, Sri Krishnadevaraya University, Anantapuramu, A.P., India,
[3]Department of Physics, SCNR Govt. Degree College, Proddatur, YSR Kadapa, A.P., India,

Abstract: In this study, the hydrothermal method has been used in the Co–Zn spinel ferrites with the chemical formula $Co_{1-x}Zn_xFe_2O_4$ ($0.1 \leq x \leq 0.9$) nanoparticles, which have been characterized using X-ray diffraction (XRD), Fourier transform Infrared spectroscopy (FTIR), UV-Vis spectrometer, and photoluminescence properties. XRD investigation confirms the cubic spinel structure and the Debye-Scherer formula was used to determine the crystallite size, showing values of 4.839 to 5.896 nm. FTIR confirms the presence of all functional groups and A, B-site wave numbers are studied and these are responsible for the characteristic of spinel ferrites. The UV-visible analysis was used to explain the variation of optical energy bandgap as Zinc doping was increased and Photoluminescence intensity was found to vary from 420-425 nm for CZF nanoparticles.

Key words **- XRD, FTIR, UV-Vis, PL and crystallite size.**

1.INTRODUCTION

Nanotechnology has revolutionized various scientific and industrial fields by offering a novel avenue for designing and engineering materials at the nanoscale. Co-Zn nanoferrite is a type of magnetic nanoparticle that has garnered significant attention in recent years due to its unique properties and potential applications in various fields. These nanoparticles are composed of cobalt (Co), zinc (Zn), and iron (Fe) oxide, with the composition Co_{1-x} $Zn_xFe_2O_4$, where x represents the Co to Zn ratio. The unique composition and structure of Co-Zn nanoferrites make them promising materials for a wide range of applications in biomedical, environmental, and industrial fields. One of the most significant advantages of Co-Zn nanoferrites is their high magnetic anisotropy, which means they have a preferred direction of magnetization. This property makes them ideal for various magnetic applications such as magnetic data storage, magnetic hyperthermia, and magnetic resonance imaging (MRI). Co-Zn nanoferrites can be used as contrast agents for MRI due to their high magnetic moment and excellent biocompatibility. Co-Zn nanoferrites have also been studied for their potential applications in the field of environmental remediation. They can be used as adsorbents for removing heavy metals and organic pollutants from water and soil due to their high surface area and magnetic properties. Additionally, they have been shown to have excellent photocatalytic activity, making them potential candidates for the degradation of organic pollutants under visible light irradiation. In the field of industrial catalysis, Co-Zn nanoferrites have been studied for their potential applications as catalysts in various chemical reactions. Due to their high surface area and unique magnetic properties, they have shown excellent catalytic activity in various reactions such as oxidation, reduction, and hydrogenation. The spinel ferrite materials are good candidates for distinct scientific and industrial fields because of their high saturation magnetization, high magnetic permeability, low electrical conductivity, and inexpensive [1]. However, these parameters mainly depend upon the type of cations, charge carriers (electrons or holes), and cationic distribution at A & B-sites

(tetrahedral & octahedral respectively) [1]. Many scientists have reported different properties including structural, optical, and magnetic, that are ideal for high-frequency applications. Therefore, these ferrite materials can be extensively useful for electromagnetic device applications [2]. In the literature it is found that several scientists worked on zinc ferrite (ZF) & cobalt ferrites (CF) and doped nanoparticles for electrical, magnetic, photocatalytic, and superparamagnetic properties [3-6]. Herein, for the synthesis of nanoparticles, citric acid worked as an added precursor along with the stoichiometric materials. In addition to these, spinel cobalt ferrite materials exhibited magnetic recording and magneto-optical recording media applications as noticed in the literature [7-10]. Therefore, the magnetic spinel structured materials preserved be expected for various technological field applications [11]. Additionally, zinc ferrite showed a normal spinel structure with an attractive structural, morphological, and magnetic properties [12]. On the other hand, the CF exhibited inverse spinel structure in nanoform [5-6]. Therefore, it can be expected that the zinc addition to the CF may reveal different electrical, magnetic, thermal, and antimicrobial properties. In addition, it was also seen that previous scientists prepared the Co-Zn ferrites in both bulks as well as nanoform via different synthesis methods such as low-temperature hydrothermal technique, starch-assisted sol-gel auto combustion method, microwave combustion method, coprecipitation method followed by high-temperature sintering, and organic solution techniques [13-17]. The obtained results of these studies were confined to only structural, optical, magnetic, cation distribution, and catalysis activity properties. Besides, the literature survey expressed the fact that the $CoFe_2O_4$ and iron oxide superparamagnetic nanomaterials were studied for magnetic hyperthermia therapy,core/shell structures, and different magnetic properties [18-24]. As a whole, this evidenced a fact that the X-ray photoelectron spectroscopy, thermal, antimicrobial, and magnetic properties were not studied at length for the Co-Zn ferrite system via the citrate gel auto combustion method. Therefore, an intention was carried out to investigate the above-mentioned properties of the Co-Zn ferrite system to advance the scientific community. The general formula Co_{1-x} $Zn_xFe_2O_4$ represents a solid solution of transition metal ferrites where the composition of cobalt (Co^{2+}), zinc (Zn^{2+}), and iron (Fe^{2+}) ions can vary systematically. The most common values of x in this formula are 0.1, 0.3, 0.5, 0.7, and 0.9, which correspond to different ratios of cobalt and zinc relative to iron. This controlled variation allows researchers to tailor the physicochemical properties of these nanoparticles to suit specific applications.

In this paper, we report the influence of Zn doping on the structural, morphological, optical, electrical, and magnetic properties of $Co_{1-x}Zn_xFe_2O_4$ nanoparticles. The substitution of non-magnetic Zn ion is expected to modify crystal as well as other properties by altering the cation distribution between the two crystallographic A and B-sites.

2. MATERIALS AND EXPERIMENTAL METHODS

For the synthesis of Co_{1-x} $Zn_xFe_2O_4$ ($0.1 \leq x \leq 0.9$)/CZF nanoparticles, we selected the starting materials as Cobalt nitrate [$Co(NO_3)_2 \cdot 6H_2O$ (99.8% purity, Sigma-Aldrich)], Zinc nitrate [$ZnN_2O_6 \cdot 6H_2O$ (99.8% purity, Sigma-Aldrich)], and ferric nitrate [$Fe(NO_3)_3 \cdot 9H_2O$ (99.9% purity, Sigma-Aldrich)]. The sodium hydroxide (NaOH) pellets and their aqueous solution were also used to work as the solvent, in the hydrothermal reaction.

At the outset, the stoichiometric equation of CZF nanoparticles was prepared as Co_{1-x} $Zn_xFe_2O_4$ ($0.1 \leq x \leq 0.9$). Using this stoichiometric formula, the raw materials (in nitrate form) were weighed on a digital sensitive balance and mixed in a fresh glass beaker. Afterward, the nitrate materials were dissolved in distilled water contained in a glass beaker. The mixed solution was then kept on a magnetic stirrer with a stirring rate of 500 rpm. In the meantime, the NaOH aqueous solution was added drop by drop to the nitrate solution. As a result of the stirring of the solution for 2 h, the white and delicious solution was obtained. This solution was further shifted to a Teflon bowl of 500 ml capacity and kept in a stainless steel autoclave. Afterward, the screws of the autoclave were made tight to prevent the explosion of the solution at the time of hydrothermal reaction. Then the autoclave was kept in a programmable hot air oven. In the oven, the hydrothermal reaction was performed at 160°C/8 h. After completion of the reaction, the oven was cooled down to room temperature. In the next step, the sample was removed from the Teflon bowl and then cleaned 10–12 times until the pH reached 7. Later on, the powder sample was dried at 60 °C for 2 h in the hot air oven. The dried CZF nanopowder was ground in an agate mortar for 15 min to achieve homogeneous powder particles.

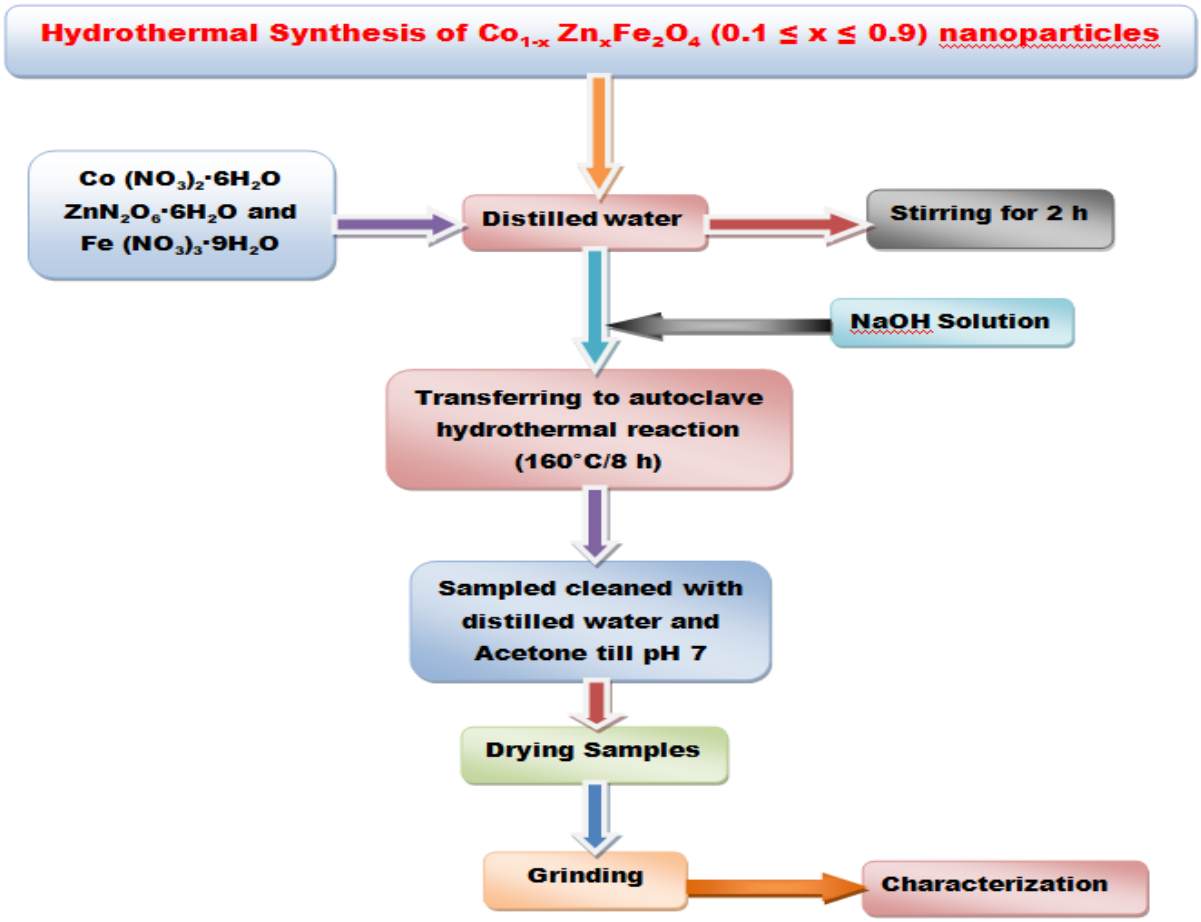

Fig.1. Flow chart for preparation of CZF nanoparticles

3. RESULTS

3.1.X-ray diffraction (XRD)

The X-ray diffraction (XRD) patterns of $Co_{1-x}Zn_xFe_2O_4$ ($0.1 \leq x \leq 0.9$) powder nanoparticles prepared are shown in Fig.2. The results showed the present CZF nanoparticles were crystal structures of cubic spinel phase. The XRD patterns were confirmed (JCPDS Number 22-1086). The diffraction pattern typically shows characteristic peaks at 2Θ values 30.1º, 35.8º, 43.2º, 47.3º, 53.7º, 56.9º, 62.7º and 68.0º. These peaks correspond to the (220), (311), (400), (331), (422), (511), (440) and (620) planes, respectively of the prepared CZF nanoparticles were cubic spinel phase [25]. Based on the diffraction peaks and using the Debye–Scherrer formula: $D = k\lambda/\beta Cos\theta$, where β is FWHM, λ is the wavelength of $Cu_{K\alpha}$ source (0.15406 nm) and θ is the diffraction angle [26-27]. The average crystalline size was found to vary from 4.839 to 5.896 nm with the increase in zinc content. It may happen microstrain ε varies from 0.0113 to 0.0412 with a doped zinc content of 'x'. The maximum intense reflection plane was noted to be (311). In addition, the lattice constants (a, b & c) were found to be equal (a = b = c) and the achieved value was observed to vary with the increase of zinc content varying from 8.329 to 8.401 Å [28-29]. This implied that the variation trend of the lattice constant obeys Vegard's law [30]. This kind of manner is obtained because of the occupation of Co^{2+} (0.58 nm) cations of smaller ionic radii by the Zn^{2+} (0.60 nm) cations of larger ionic radii [31]. Subsequently, the unitcell volume (V) was also increased from 577.97 to 591.31 $Å^3$. This indicated the fact that the expansion of the unit cell took place in the CZF nanoparticles with Zn-content. Besides, the X-ray density (ρ_x) of CZF nanoparticles was found to vary from 5.34 to 5.41 g/cm^3 using the formula: ZM/Na^3, herein 'Z' indicates the effective number of atoms per unit cell (8), 'M' is associated to the compositional molecular weight, 'N' is the Avogadro's number and 'a' is lattice parameter of content[32]. The present behavior of ρ_x is obtained as a result of the decrease of molecular weight with an increase in zinc concentration. Moreover, this kind of nature was noticed in the literature [33]. In a few cases, the linear increase of 'a' with Zn-content can also be expected as another reason for the behavior of X-ray density [34]. The bulk density (ρ_b) of CZF nanoparticles was estimated to vary from 4.021 to 4.071 g/cm^3 using equation $\rho_b = M/\Pi r^2 h$. Further, the porosity of the CZF nanoparticles was found to vary from 0.2469 to 0.2477 using the equation: Porosity (P %) = $[1- (\rho_x / \rho_b)] *100$. The CZF nanoparticles were determined dislocation density (ρ) varying from 2.877E+16 to 4.271 E+16 m^{-2}, a specific surface area (S) varying from 190.57 to 231.76 m^2/g listed in Table 1.

3.2.WILLIAMSON- HALL ANALYSIS

To calculate approximately the strain and crystallite size, we have preferred the W-H plot for CZF nanoparticles shown in Fig.3 and expressed in equation [35]: $B\,Cos\Theta = \frac{K\lambda}{D} + 4\varepsilon\,Sin\Theta$, Where λ= wavelength, β=Full-Width Half Maxima (FWHM), Θ= Bragg's diffraction angle, ε= Micro-strain and D= crystallite size. The slope of the W-H plot gives the Micro-strain value. The CZF nanoparticles Micro-strain ($\varepsilon_{W\text{-}H}$) varied from 0.0299 to 0.0519 and the crystallite size ($D_{W\text{-}H}$) was calculated to be varying from 2.679 to 4.62 nm of zinc content 'x'. The average crystallite sizes estimated by the two methods are close to each other. Further, a good agreement is perceived between the values expressed from the W-H Plot based on Scherrer's formula and the values $\varepsilon_{W\text{-}H}$ and $D_{W\text{-}H}$ in Table 1. [36].

1.1.OPTICAL PROPERTIES

FTIR spectra of $Co_{1-x}\,Zn_xFe_2O_4$ ($0.1 \leq x \leq 0.9$), the sample codes are C1, C2, C3, C4, and C5 of room temperature in a wave number range from 400 to 4500 cm^{-1} are represented in Fig.4. All FTIR spectra in the described range demonstrate two well-defined peaks, first one around 462.72 cm^{-1} to 475.03 cm^{-1} (υ_b) and the other near 539.67 cm^{-1} to 557.11 cm^{-1} (υ_a), which are related to intrinsic stretching. The metal-oxygen (M-O) vibration bands like Co-O, Zn-O & Fe-O can be noticed in CZF samples [36] as it is known that theZn^{2+}, Fe^{3+}, Co^{2+} ions can occupy both A and B-sites of spinel structure [1]. Vibrations of the oxygen bond with metal cations in positions of the tetrahedral sites (A- sites) and the octahedral sites (B-sites). The weak frequency peak (υ_b) attributed to the intrinsic vibration of the metal-oxygen bond at the B- sites and the high-frequency peak (υ_a) shown the metal-oxygen vibration of the A- sites [37] are shown in Fig.4.

Table 1. Data on the XRD structural and physical parameters of CZF nanoparticles

Parameters	C1 (x=0.1)	C2 (x=0.3)	C3 (x=0.5)	C4 (x=0.7)	C5 (x=0.9)
Lattice Parameter (a)	8.329	8.374	8.372	8.401	8.397
Crystallite size(D_{ave}) in nm	4.886	4.839	4.840	5.896	5.582
Strain ε	0.0412	0.0354	0.0173	0.0113	0.0128
$D_{W\text{-}H}$	4.62	2.679	3.136	3.044	4.09
$\varepsilon_{W\text{-}H}$	0.0299	0.0517	0.044	0.045	0.0339
FWHM in radians	0.04747	0.0596	0.0265	0.0235	0.0240
Volume V (A^{o3})	577.97	587.35	587.62	594.72	592.31
MW g/mol	235.265	236.55	237.84	239.13	240.42
Surface Area S (m^2/g)	226.98	231.76	230.42	190.57	199.42
Dislocation density (m^{-2})	4.189 E+16	4.271 E+16	4.269 E+16	2.877 E+16	3.209 E+16

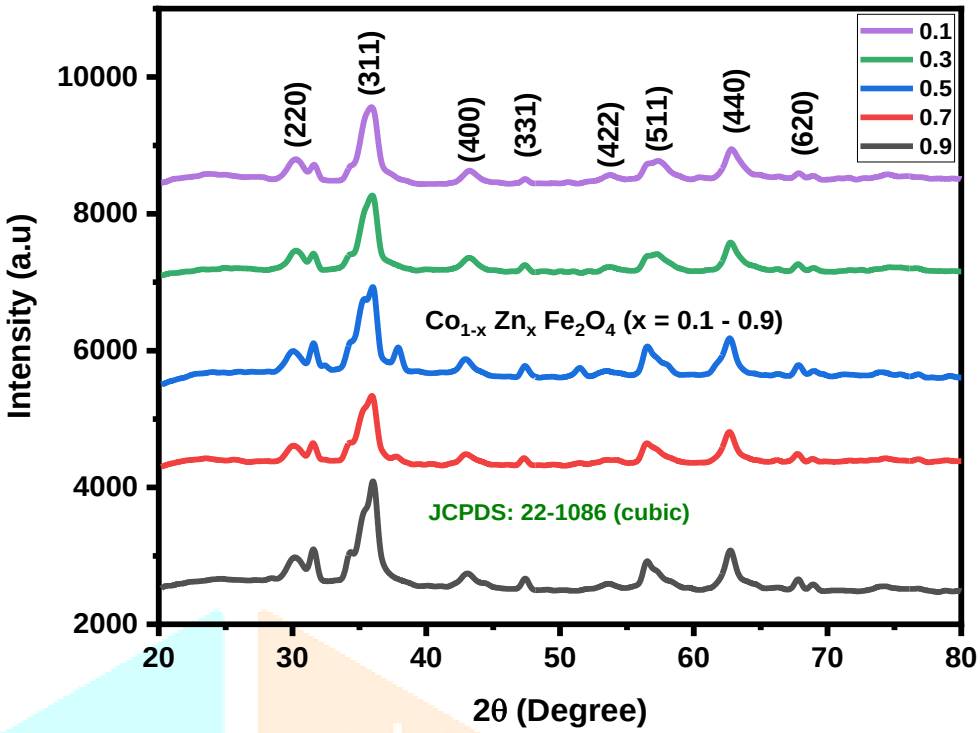

Fig.2. X-ray diffraction (XRD) pattern of CZF nanoparticles

To calculate the optical energy gap (E_g), the Kubelka-Munk function was considered. Using this, the function of reflectance F(R): $(1\text{-}R)^2/2R$, (where R = reflectance which was recorded from diffuse reflectance spectra as shown in the inset of Fig.5) was computed [33]. Here, the F(R) was observed to be directly proportional to the absorptivity (α), and therefore, in place of 'α', we can substitute F(R). Further, using the equation: $(\alpha h\nu)^n = m\ (h\nu - E_g)$ and the $(\alpha h\upsilon)^n$ versus photon energy (hυ) plots, we calculated the E_g values of CZF. The exponent (n) in the band gap equation was taken as 2 for the direct transition of charge carriers between two energy bands [33, 38]. The $(\alpha h\upsilon)^n$ versus hυ plots of x = 0.1-0.9 contents showed the linear portions. The linear portion was extrapolated towards the hυ-axis. Then, using the intersecting position of the straight line at the hυ-axis, wherein α approaches zero, the E_g values were calculated. These E_g values were indexed in Fig.4. The results indicated that the E_g values were varying from 0.935 to 1.524 eV with an increase of Zn-content from x = 0.1 to 0.9. This kind of behavior is mainly attributed to the oxygen vacancies present in each composition. That is, the E_g value will be high for the lower number of oxygen vacancies and vice versa [38]. In the case of CZF nanoparticles, the numbers of oxygen vacancies were varying with the increase of Zn-content. Therefore, the concerned distance between the valence and conduction bands was varied (from 0.935 to 1.524 eV). However, the x = 0.1-0.9 contents showed wide E_g values suggesting optoelectronic and sensor applications [38].

The photoluminescence spectra were found in the visible region and were independent of the particle size. The PL spectra of $Co_{1-x}\ Zn_xFe_2O_4$ ($0.1 \leq x \leq 0.9$) /CZF nanoparticles are shown in Fig.6. The Photoluminescence intensity was found varying from 420-425 nm for CZF nanoparticles. The most well-known peaks in visible regions were only one which is dependent on particle size. The PL emission of light from a material under optical excitation is an essential trend. If light of sufficient energy is incident on a material, photons are absorbed important near electronic excitations. These excitations then relax and the electrons return to the ground state. Photoluminescence occurs when the radiative relaxation occurs. Since the excitation wavelength might impact the photoluminescence of any material, the absorption of a material depends strongly on the energy of an incident light. This makes the selection of the excitation light consequently critical in the photoluminescence study of material. The excitation wavelength controls a density of photo-excited electrons and holes and this governs the behavior of these carriers. Here, the photoluminescence spectrums of CZF nanoparticles at room temperatures have been observed at the excitations varying from 420nm - 425nm. The spectrum consists of emission peaks varying from 420 nm (2.95 eV) - 425 nm (2.92 eV). It is also observed that the emission intensity of the peaks depends on the excitation wavelength. Concerning the mechanism of PL, it may be attributable to quantum confinement. This

confinement can be explained in terms of the shortening of a super-exchange interaction bond length in the nano-crystalline ferrite materials, which modifies the electronic structure of ferrite, or in terms of the occurrence of the fast non-radiative relaxation channels in nano-crystals which are enchanting part at the surface. The PL around 3 eV is indeed generally due to quantum confinement although the peak values approximately agree with an energy band gap of ferrite nanomaterials. The effect of the surface oxide and non-homogenous size was furthermore important if there is a difference within the energies, which is associated with the Stokes shift between the absorption surface defects or surface oxide. The mechanism of the charge transfer between the trivalent ions appears to involve a non-radiative super-exchange process via the intervening oxide ions that support the ferromagnetic ordering [39]. The PL is such that their intrinsic and extrinsic bands were within the visible range [40].

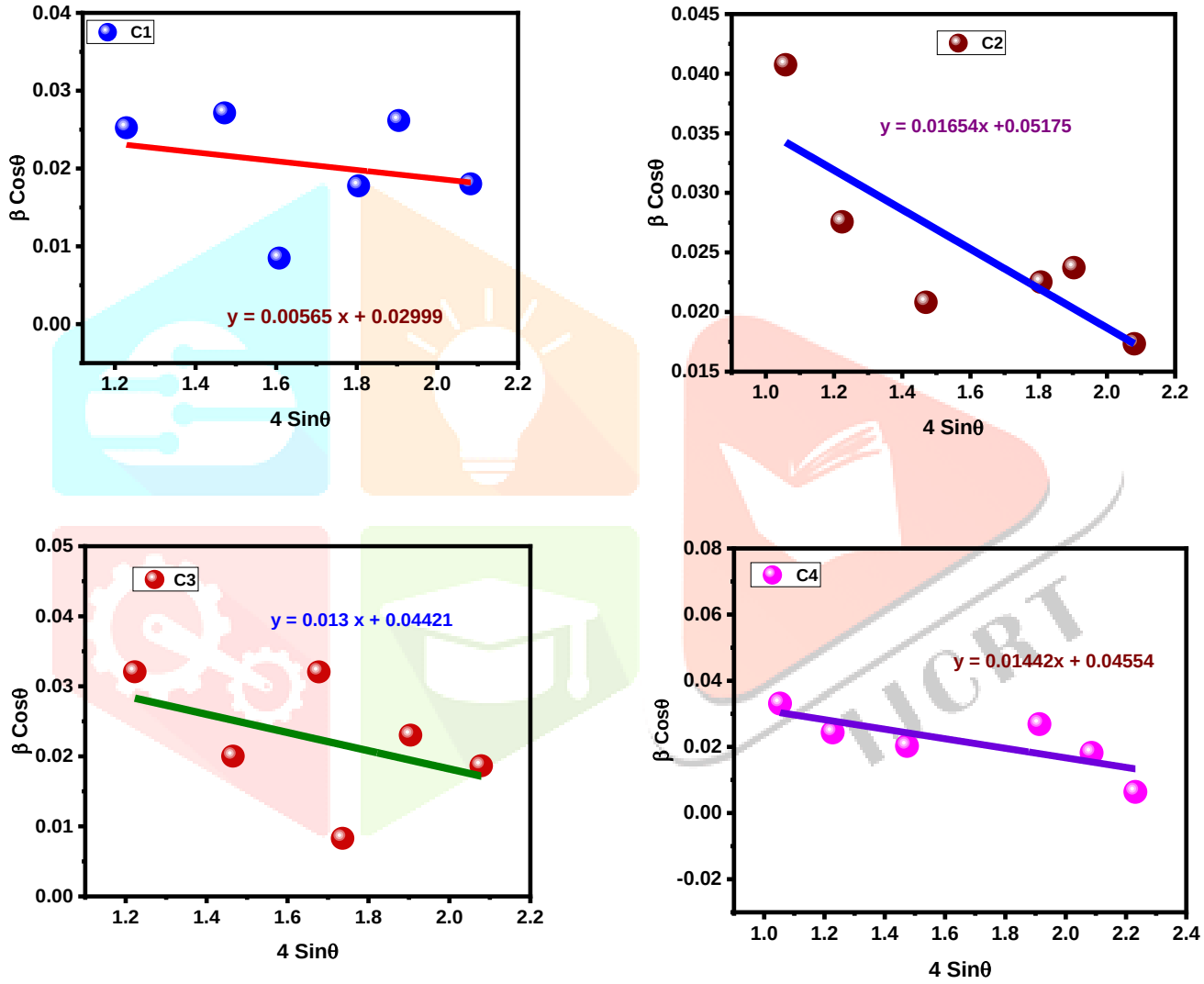

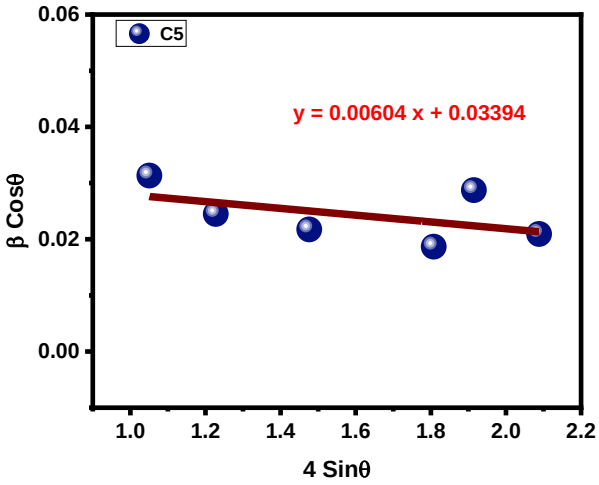

Fig.3. W-H Plot of CZF nanoparticles

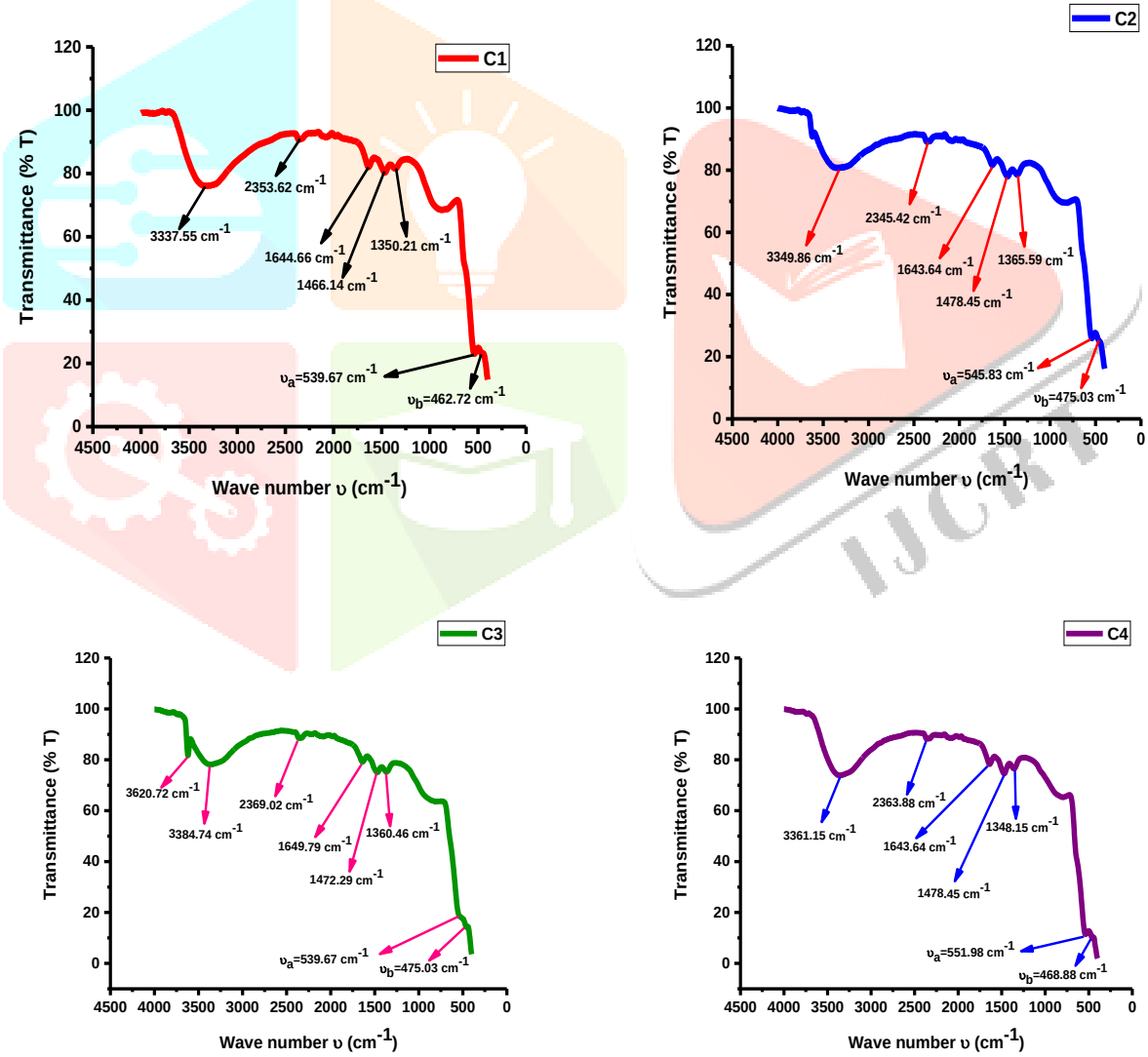

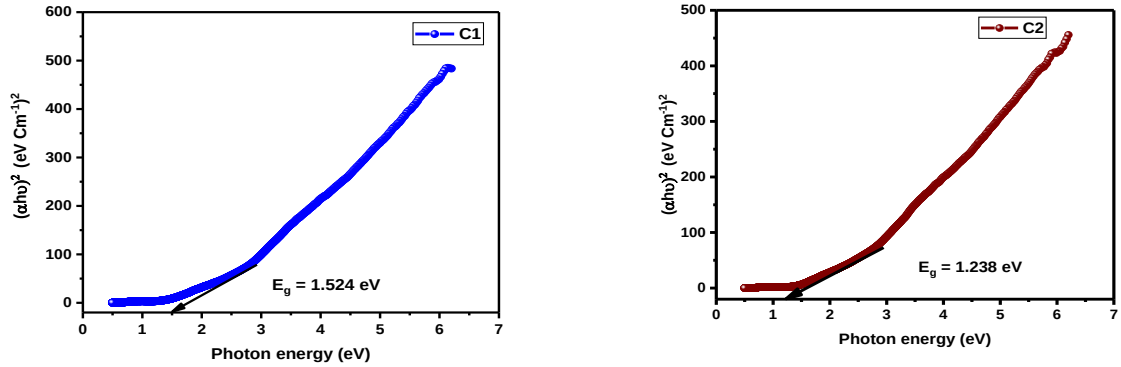

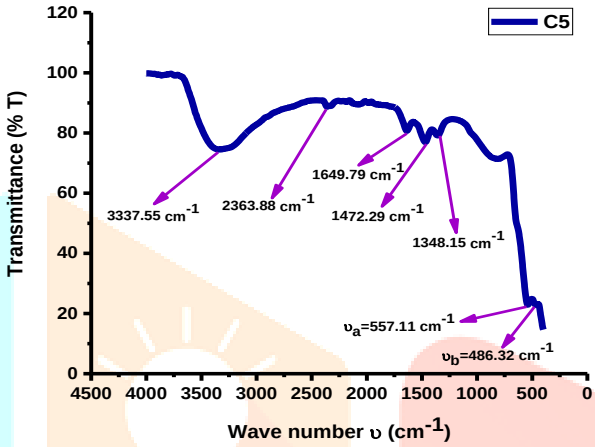

Fig.4. FTIR plots of CZF nanoparticles

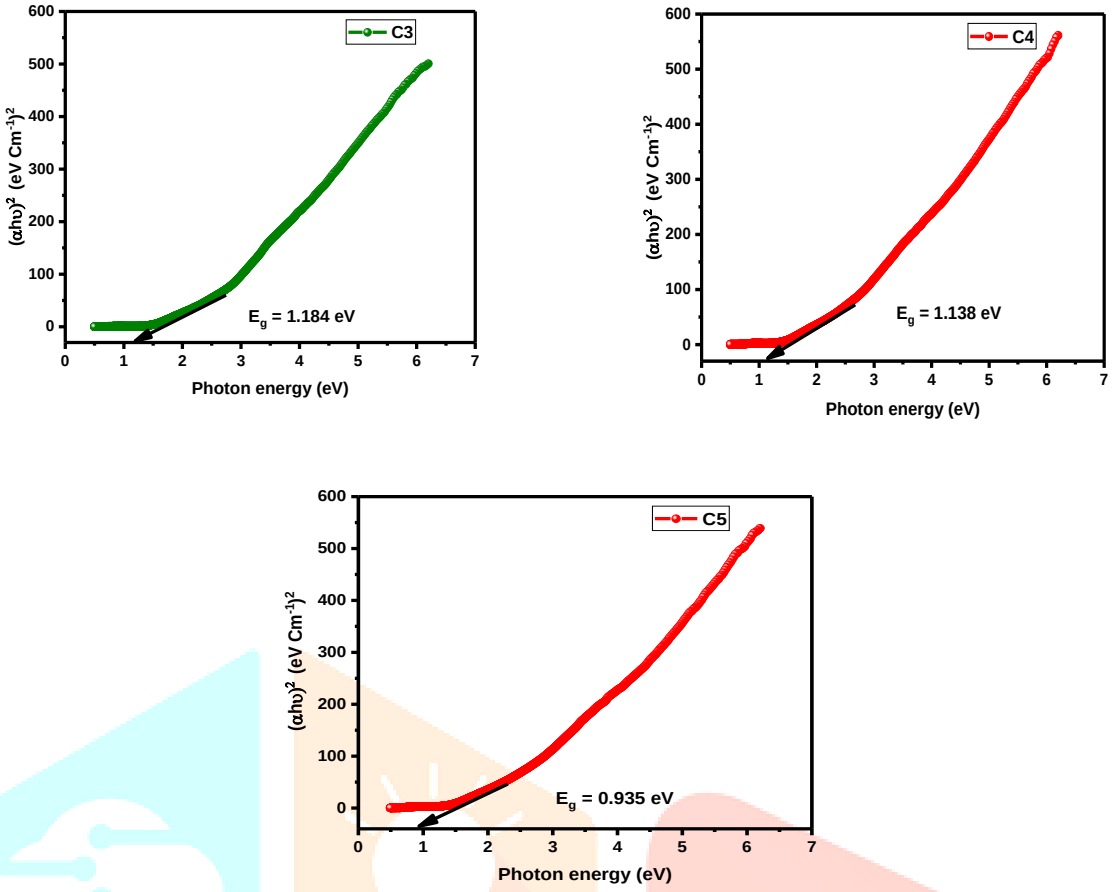

Fig.5. UV-Vis spectra of CZF nanoparticles

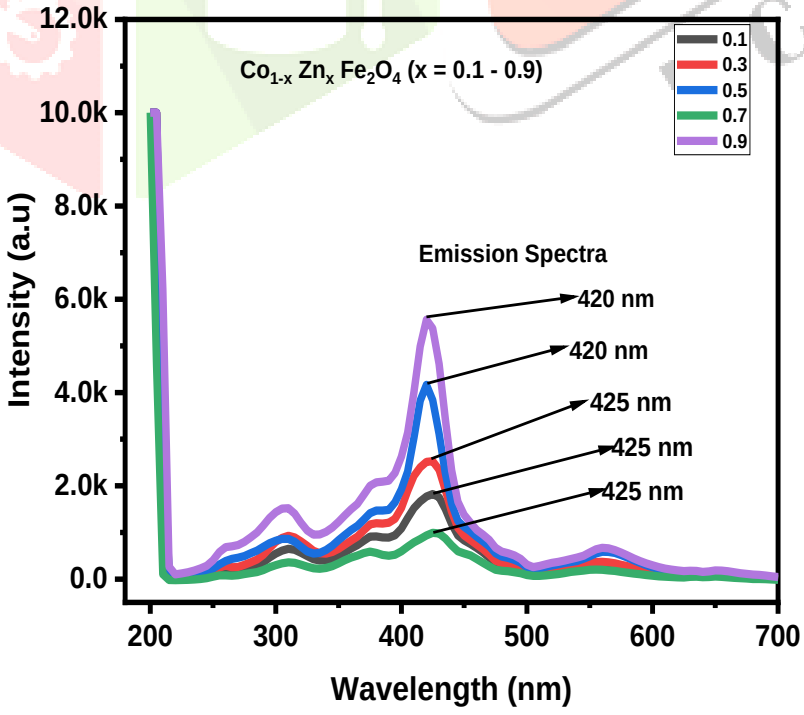

Fig.6. PL spectra of CZF nanoparticles

2. CONCLUSIONS

The hydrothermal method is found to be successful in the preparation of the spinel ferrite $Co_{1-x}Zn_xFe_2O_4$ ($0.1 \leq x \leq 0.9$) nanoparticles. The XRD has confirmed the formation of a cubic spinel structure. The lattice constants (a=b=c) vary from 8.329 to 8.401 Å with an increase in zinc content. Using Scherrer's formula and W-H analysis, the average crystallite size and the lattice strains were determined, and average crystallite sizes estimated by the two methods are close to each other. Two main absorption peaks in the range from 462.72 cm^{-1} - 475.03 cm^{-1} (υ_b) for octahedral sites, and the range 539.67 cm^{-1} to 557.11 cm^{-1} (υ_a) for tetrahedral sites observed in FTIR spectra which confirmed the ferrite nature of the sample. The intense emissions of 420nm - 425nm occurred mainly due to radiative defects and oxygen vacancies in the room-temperature PL studies. The energy band gap of prepared samples was calculated from varying between 0.935 to 1.524 eV with increasing Zn content 'x'. These $Co_{1-x}Zn_xFe_2O_4$ ($0.1 \leq x \leq 0.9$) nanoparticles are promising for suggesting optoelectronic and sensor applications.

3. ACKNOWLEDGMENTS

The authors expressed thankfulness to Dr. M. V. Lakshmaiah, Professor (Physics & Electronics), Department of Physics, Sri Krishnadevarya University, Ananthapuramu, for providing Research Lab, My special thanks go to SRMIST consultancy, SRM University, Chennai for providing me the necessary characterizations (FTIR, and UV-Vis), XRD and PL providing Yogi Vemana University, YSR Kadapa and IISc, Bangalore, respectively.

REFERENCES

1. Nehru Boda, Gopal Boda, Chandra Babu Naidu K, Srinivas M, Khalid Mujasam Batoo, Ravinder D et al. Effect of Rare Earth Elements on Low-Temperature Magnetic Properties of Ni and Co-Ferrite Nanoparticles, Journal of Magnetism and Magnetic Materials, 2019; 473: 228-235
2. Aravind G, Raghasudha M, Ravinder D, Manivel Raja M, Meena S S, Pramod Bhatt, et al. Study of structural and magnetic properties of Li–Ni nano ferrites synthesized by citrate-gel auto combustion method, Ceramics International, 2016; 42: 2941-2950
3. Manohar A, Krishnamoorthi C, Magnetic and photocatalytic studies on $Zn_{1-x}Mg_xFe_2O_4$ nano colloids synthesized by solvothermal reflux method, Journal of Photochemistry and Photobiology B: Biology, 2017;177: 95-104
4. Manohar A, Krishnamoorthi C, Photocatalytic study and superparamagnetic nature of Zn-doped $MgFe_2O_4$ colloidal size nanocrystals prepared by solvothermal reflux method, Journal of Photochemistry and Photobiology B: Biology, 2017; 173: 456-465
5. Islam MU, Rana MU, Abbas T, Study of Magnetic Interactions in Co-Zn-Fe-O System, Mater Chem Phys, 1998; 57: 190-193.
6. Hemeda OM, Abd El-Ati MI, Spectral Studies of $Co_{0.6}Zn_{0.4}$ Fe_2O_4 at Different Soaking Times, Materials Letters, 2001; 51: 42-47.
7. Suzuki Y, van Dover RB, Gyorgy EM, Philips JM, Korenivski J, Werder J, et al. Structure and magnetic properties of epitaxial spinel ferrite thin films, Appl Phys Lett, 1996; 68: 714-716.
8. Cheng FX, Jia JT, Xu ZG, Zhou B, Liao CS, Yan CH et al. Microstructure, magnetic, and magneto-optical properties of chemically synthesized Co-RE(RE = Ho, Er, Tm, Yb, Lu)ferrite nanocrystalline films, J Appl Phys, 1999; 86: 2727-2732.
9. Kitamoto Y, Kantake S, Shirasaki A, Abe F, Naoe M. Co ferrite films with excellent perpendicular magnetic anisotropy and high coercivity deposited at low temperature, JAppl Phys 1999; 85: 4708-4710.
10. Fontijn WFJ, vander Zaag PJ, Feiner LF, Metselaar R, Devillers MCA. A consistent interpretation of the magneto-optical spectra of spinel type ferrites, J Appl Phys, 1999; 85: 5100-5105.
11. Bettinger JS, Chopdekar RV, Liberati M, Neulinger JR, Zhshiev M, Akamwa Y., magnetism and transport of $CuCr_2Se_4$ thin films, J Magn Magn Mater, 2007; 318: 65- 73.
12. Chinnasamy CN, Narayanasamy A, Ponpandian N, Chattopadhyay K, Guerault H, Grenache JM, Magnetic properties of nanostructured ferrimagnetic zinc ferrite, J Phys condensed Matter, 2000; 12: 7795-7805.
13. Phong P T, Nam P H, Phuc N X, Huy B T, Lu L T, Manh D H et al. Effect of Zinc Concentration on the Structural, Optical, and Magnetic Properties of Mixed Co-Zn Ferrites Nanoparticles Synthesized by Low-Temperature Hydrothermal Method, Metallurgical and Materials Transactions A, 2019; 50: 1571-1581
14. Yadav Raghvendra Singh, Havlica Jaromir, Hnatko Miroslav, Šajgalík Pavol, Alexan der Cigáň Palou Martin, Bartoníčková Eva et al. Magnetic properties of $Co_{1-x}Zn_xFe_2O_4$ spinel ferrite

nanoparticles synthesized by starch-assisted sol-gel auto combustion method and its ball milling, Journal of Magnetism and MagneticMaterials, 2015; 378: 190-199.

15. Manikandan A, John Kennedy L, Bououdina M, Judith Vijaya J, Synthesis, optical and magnetic properties of pure and Co-doped $ZnFe_2O_4$ nanoparticles by microwave combustion method, Journal of Magnetism and Magnetic Materials, 2015; 378: 190- 199.
16. Veverka M, Jirak Z, Kaman O, Knızek K, Marysko M, Pollert E et al. Distribution of cations in nanosize and bulk Co–Zn ferrites, Nanotechnology 2011; 22: 345701 (7pp)
17. Thurpu Raghavender Reddy, Dodla Sivanageswara Rao and Sudhir Kashyap A, mild and efficient Zn-catalyzed *C*-glycosylation: synthesis of C(2)–C(3) unsaturated *C*-linked glycopyranosides, RSC Adv**.,** 2015; 5: 28338-28343
18. Zohreh Nemati, Javier Alonso, Irati Rodrigo, Raja Das, Eneko Garaio, José Ángel García et al. Improving the Heating Efficiency of Iron Oxide Nanoparticles by TuningTheir Shape and Size, J. Phys. Chem. C., 2018; 122: 2367–2381
19. Phong P T, Phuc N X, Nam P H, Chien N V, Dung D D, Linh P H, Size-controlledheating ability of $CoFe_2O_4$ nanoparticles for hyperthermia applications, Physica B: Physics of Condensed Matter, 2018; 531: 30-34
20. Zohreh Nemati Porshokouh, Salili S M, Alonso J, Ataie A, Das R, Phan M H et al. Superparamagnetic iron oxide nanodiscs for hyperthermia therapy: Does size matter?,Journal of Alloys and Compounds, 2017; 714: 709-714
21. Das R, Rinaldi-Montes N, Alonso J, Amghouz Z, Garaio E, García J A et al. Boosted Hyperthermia Therapy by Combined AC Magnetic and Photothermal Exposures in Ag/Fe_3O_4 Nanoflowers, ACS Appl. Mater. Interfaces, 2016; 8: 25162– 25169
22. Raja Das, Javier Alonso, Zohreh Nemati Porshokouh, Vijayasankar Kalappattil, David Torres, Phan M H et al. Tunable High Aspect Ratio Iron Oxide Nanorods for Enhanced Hyperthermia, Journal of Physical Chemistry C, 2016; 18: 10086-10093
23. Peddis D, Cannas C, Musinu A, Ardu A, Orrù F, Fiorani D et al. Beyond the Effect of Particle Size: Influence of $CoFe_2O_4$ Nanoparticle Arrangements on Magnetic Properties, Chem. Mater., 2013; 25: 2005–2013
24. Manh-Huong Phan, Javier Alonso, Hafsa Khurshid, Paula Lampen-Kelley, Sayan Chandra, Kristen Stojak Repa, et al. Exchange Bias Effects in Iron Oxide-Based Nanoparticle Systems, Nanomaterials, 2016; 6: 221
25. Cullity B. D. Elements of X-ray diffraction, 2nd ed. Addison-Wesley, Reading, MA, 1978
26. Kumar N S, Suvarna R P, Naidu K C B, Sol-Gel Synthesized and Microwave Heated $Pb_{0.8-y}La_yCo_{0.2}TiO_3$ (y= 0.2–0.8) Nanoparticles: Structural, Morphological and Dielectric Properties, Ceramics International, 2018; 44: 18189-18199
27. Murth SR, Seshagiri Rao T, Effect of magnetic field and temperature on the elastic behavior of Co Zn ferrites, J Less-Common Met., 1979; 65: 19-26.
28. Murth SR, Dielectric behavior of Co-Zn ferrites, J. Mater Sci Lett., 1984; 3: 1049- 1051.
29. Abd El-Ati MI, Kafafy MA, Tawfik A, Magnetic properties of zinc doped ferrites, Acta Phys Pol A., 1991; 79: 889-894.
30. Vegard L, Die Konstitution der Mischkristalle und die Raumfüllung der Atome, Zeitschrift für Physik a Had-rons and Nuclei, 1921; 5: 17-26.
31. Shannon R D, Revised Effective Ionic Radii and Systematic Studies of Interatomic Distances in Halides and Chalcogenides, Acta Cryst A, 1976; 32: 751-767.
32. Hashim M, Raghasudha M, Jyoti Shah, Sagar Shirsath E, Ravinder D, Shailendra Kumar et al. High-temperature dielectric studies of indium-substituted NiCuZn nano ferrites, Journal of Physics and Chemistry of Solids, 2018; 112: 29-36
33. Kothandan D, Kumar R J, Prakash M, Naidu K C B, Structural, morphological and optical properties of $Ba_{1-x}Cu_xTiO_3$ (x = 0.2, 0.4, 0.6, 0.8) nanoparticles synthesized by hydrothermal method, Materials Chemistry and Physics 2018; 215: 310–315
34. Smit J, Wijn HPJ, Ferrites-Physical Properties of Ferrimagnetic Oxides about their Technical Applications, Ferrites, John Wiley, New York, 1959.
35. U. Naresh, RJ Kumar, KCB Naidu, Hydrothermal synthesis of barium copper ferrite nanoparticles: Nanofiber formation, optical, and magnetic properties, Materials Chemistry and Physics, 2019, 121807.

36. S Dastagiri, MV Lakshmaiah, V.Manjunath, NNK Reddy, KC Mohan, et al, Investigation on functional properties of $Al_{0.8}Eu_yLa_{0.2-y}TiO_3$ (y=0.01 - 0.04) nanoparticles synthesized by hydrothermal method, Surface Review, and Letters, 2022, 2250097.
37. Parvin Imanipour, Saeed Hasani, Md. Afshari, et al., The effect of divalent ions of zinc and strontium substitution on the structural and magnetic properties on the cobalt site in cobalt ferrite, Journal of Magnetism and Magnetic Materials, 2020, 166941.
38. M.H.Jameel, M.A.Agam, M.Q.Hamzah et al, Structural, optical and morphological properties of zinc –doped cobalt – ferrites $CoFe_{2-x}$ Zn_xO_4 (x=0.1-0.5), Digest Journal of Nanomaterials and Biostructures, 2021, 399-408.
39. Shashank Bhushan Das, RK Singh, V.Kumar, et al, Structural, magnetic, optical and ferroelectric properties of Y^{3+} substituted cobalt ferrite nanomaterials prepared by a cost-effective sol-gel route, Materials Science in Semiconductor Processing, 2022, 106632.
40. D. Chinna Venkata Subbaiah, S Dastagiri, G. Pakardin, et al, Synthesis And Investigation of Cobalt Ferrite Nanoparticles: Structural, Morphological, Optical, Magnetic, and Dielectric Properties, International Journal of Engineering Research & Technology, 2023, 13-21.